

Transcriptional and Functional Changes of the Human Microvasculature during Physiological Aging and Alzheimer Disease

Simone Bersini, Rafael Arrojo e Drigo, Ling Huang, Maxim N. Shokhirev, and Martin W. Hetzer*

Aging of the circulatory system correlates with the pathogenesis of a large spectrum of diseases. However, it is largely unknown which factors drive the age-dependent or pathological decline of the vasculature and how vascular defects relate to tissue aging. The goal of the study is to design a multianalytical approach to identify how the cellular microenvironment (i.e., fibroblasts) and serum from healthy donors of different ages or Alzheimer disease (AD) patients can modulate the functionality of organ-specific vascular endothelial cells (VECs). Long-living human microvascular networks embedding VECs and fibroblasts from skin biopsies are generated. RNA-seq, secretome analyses, and microfluidic assays demonstrate that fibroblasts from young donors restore the functionality of aged endothelial cells, an effect also achieved by serum from young donors. New biomarkers of vascular aging are validated in human biopsies and it is shown that young serum induces angiopoietin-like-4, which can restore compromised vascular barriers. This strategy is then employed to characterize transcriptional/functional changes induced on the blood–brain barrier by AD serum, demonstrating the importance of PTP4A3 in the regulation of permeability. Features of vascular degeneration during aging and AD are recapitulated, and a tool to identify novel biomarkers that can be exploited to develop future therapeutics modulating vascular function is established.

1. Introduction

The recent discovery that vascular endothelial cells (VECs) exhibit organ-specific molecular markers^[1,2] has sparked new interest on the role of the vascular endothelium in aging and multiple age-related diseases, including neurodegeneration,^[3] osteoporosis,^[4] stem cell exhaustion,^[5] and skin photoaging.^[6] In vivo studies demonstrated that both endothelial-supporting cells (e.g., pericytes, fibroblasts)^[7] and circulating molecules (e.g., GDF11)^[8] play a critical role in the homeostasis and aging of VECs and tissues. For example, parabiosis experiments showed improved functionality of the cerebral vasculature of aged mice, coupled with increased activation of neural stem cell proliferation and neurogenesis.^[8] However, our understanding of the molecular factors of the microenvironment and serum that promote or potentially revert human vascular aging during physiology and disease is still rudimentary.

Cerebrovascular pathologies (e.g., microinfarcts, hemorrhage, atherosclerosis)

are intimately linked to neurodegeneration and aging. It is now established that the appearance of vascular dysfunction occurs before the onset of cognitive impairment and the detection of traditional Alzheimer disease (AD) biomarkers.^[9–11] Indeed, AD patients often exhibit cerebral amyloid angiopathy and dysregulated gene expression in the blood vessels of the brain, referred to as blood–brain barrier (BBB). Intriguingly, these gene expression changes are also seen during normal aging and in early-stage AD before amyloid deposition and brain atrophy are evident. Furthermore, we have recently found that VECs forming the BBB are extremely long-lived, being as old as neurons.^[12] Because of their extreme longevity, VECs are susceptible to functional deterioration over time due to the long-term exposure to toxic metabolites, oxidative stress, and protein aggregates. Thus, it is important to analyze changes in the vasculature during normal aging and AD in order to determine their effects on healthy and pathological brain function.

Targeting vascular dysfunction in the BBB might represent a promising approach to block the early signs of the disease and to delay or even prevent cognitive impairment. Accordingly,

Dr. S. Bersini, Dr. R. Arrojo e Drigo, Prof. M. W. Hetzer
Molecular and Cell Biology Laboratory
The Salk Institute for Biological Studies
10010 North Torrey Pines Road, La Jolla, CA 92037, USA
E-mail: hetzer@salk.edu

Dr. S. Bersini
Paul F. Glenn Center for Biology of Aging Research at The Salk Institute
10010 North Torrey Pines Road, La Jolla, CA 92037, USA

Dr. L. Huang, Dr. M. N. Shokhirev
The Razavi Newman Integrative Genomics and Bioinformatics Core (IGC)
The Salk Institute for Biological Studies
10010 North Torrey Pines Road, La Jolla, CA 92037, USA

 The ORCID identification number(s) for the author(s) of this article can be found under <https://doi.org/10.1002/adbi.202000044>.

© 2020 The Authors. Published by WILEY-VCH Verlag GmbH & Co. KGaA, Weinheim. This is an open access article under the terms of the Creative Commons Attribution-NonCommercial-NoDerivs License, which permits use and distribution in any medium, provided the original work is properly cited, the use is non-commercial and no modifications or adaptations are made.

DOI: 10.1002/adbi.202000044

oxidative stress in AD can induce pericyte contraction leading to vessel hypoperfusion,^[13] hence demonstrating a potential vascular therapeutic target.

In vivo^[14] and in vitro^[15] models have contributed to the discovery of mechanisms related to vascular aging and dysfunction. For instance, senescence of VECs was reported to induce BBB breakdown in vitro.^[16] However, simplified 2D in vitro approaches do not recapitulate the complexity of the physiological 3D multicellular microenvironment. At the same time, while in vivo preclinical models play an irreplaceable role in testing the effects of drugs in a living organism, recent evidences suggest that unpredicted toxicity^[17] could only be detected through human cell-based models mimicking the physiological architecture and functionality of tissues.^[18]

To fill this gap, 3D multiculture systems have been developed to study the role of biophysical and biochemical stimuli, including cell–cell and cell–matrix communications, on the pathophysiology of complex cellular systems. For instance, the complexity of the neurovascular unit was recapitulated within microfluidic devices to elucidate the metabolic coupling between VECs and brain cells^[19] as well as the disruption of the vascular barrier integrity in presence of amyloid beta-expressing cells^[20] or cells derived from patients with Huntington disease.^[21]

Here, we describe the design and validation of a multianalytical strategy to identify and then modulate the signatures of VEC dysfunction during physiological aging and AD. More in detail, we focused on the contribution of the cellular microenvironment and serum obtained from donors of different ages as well as from AD versus age-matched healthy donors. We first validated our strategy in a skin microvasculature model by comparing the in vitro identified signature of vascular aging with human biopsies from donors of different ages. We then applied our validated approach to the study of the transcriptional and functional changes occurring in the BBB during AD, revealing new potential biomarkers for the early detection of vascular dysfunction and for its therapeutic correction.

2. Results

2.1. Design and Characterization of an In Vitro 3D Model of Long-Living Skin Microvasculature

The skin microvasculature is known to undergo age-related decline which is linked to the onset of several pathological conditions including stasis dermatitis and angioma. The human skin microvasculature is composed of capillary vessels formed by endothelial cells that are partially wrapped by supporting mural cells (e.g., smooth muscle cells, pericytes) and surrounded by a network of collagen-secreting fibroblasts. In order to recapitulate this basic organization, we cocultured dermal microvascular ECs (dVECs) and fibroblasts obtained from skin biopsies within 3D fibrin scaffolds. After 25 d in the presence of serum, dVECs self-assembled into capillary vessels surrounded by collagen type I secreting fibroblasts (Figure S1A–F, Supporting Information). In addition, a subpopulation of fibroblasts differentiated into a smooth muscle cell-like phenotype and partially wrapped the capillary network (Figure S1G, Supporting Information). To obtain quantitative features

of this system, we monitored the remodeling of the network over 25 d and quantified vascular density (Figures S1A,B and S2A, Supporting Information), collagen type I deposition (Figures S1C,D and S2B, Supporting Information), cell proliferation (Figures S1E,F,H,I and S2C–E, Supporting Information), and mural cell localization (alpha smooth muscle actin, Figure S2F,G, Supporting Information). Together, these observations highlighted a dynamic environment which is self-organizing and maturing toward a simplified skin microvascular unit.

Moreover, we quantified the expression of p16, a well-known senescence marker (Figure S2H,I, Supporting Information). Less than 1% cells were p16 positive, suggesting that senescence does not play a major role in the in vitro system. Of note, in vivo observations also suggest that only a small percentage of cells (<8%) senesce in aging skin. No signs of increased apoptosis over time were detected. Finally, the 3D vascular model also produced and remodeled the extracellular matrix (ECM) (Figure S2J, Supporting Information) and formed open-lumen structures (Figure S2J,K, Supporting Information). Overall, we designed and characterized a long-living model of the skin microvasculature which recapitulates key features of the basic vascular unit observed in vivo such as low proliferation rates and low abundance of senescence cells.

2.2. Fibroblasts from Young Donors Restore the Functionality of an Aged Endothelium

Previous studies reported that fibroblasts from aged donors secrete a wide range of aging-associated proteins^[22] and that their signature can be maintained when transdifferentiated into other cell types.^[23] Having established a 3D model that faithfully recapitulates key features of the skin microvasculature, we wanted to test whether the function of dVECs could be modulated by fibroblasts isolated from individuals with different chronological age.

First, we tested if fibroblasts from young individuals could restore the functionality of old dVECs. We cocultured dVECs from an old donor (age 66 years old) with skin fibroblasts collected from young (age range 19–34 years old) or old (age range 63–69 years old) patients ($N = 5$ donors per age group) (Table S1, Supporting Information). The donors were reported to be Caucasian, nondiabetic, nonsmokers, and without any medical issue. While we did not observe significant changes in other vascular parameters including vessel diameter and collagen deposition (Figure S3, Supporting Information), the density of the vascular network was higher in presence of fibroblasts from old donors (OFs) when compared to young donors (YFs) (Figure S3A,B, Supporting Information). In addition, vascular density changes were not correlated with the onset of senescence, since p16 positive cells were detected in both young and old microenvironments, again suggesting that senescence does not influence the results obtained with our model. Importantly, a fully developed basement membrane (BM) surrounding the vessels only formed with YFs (Figure 1A and Figure S4, Supporting Information). The presence of a continuous BM is a sign of vascular maturation and represents one of the key features to generate physiological blood vessels.

We hypothesized that the observed structural changes caused by OFs (i.e., increased vascular density, impaired BM deposition)

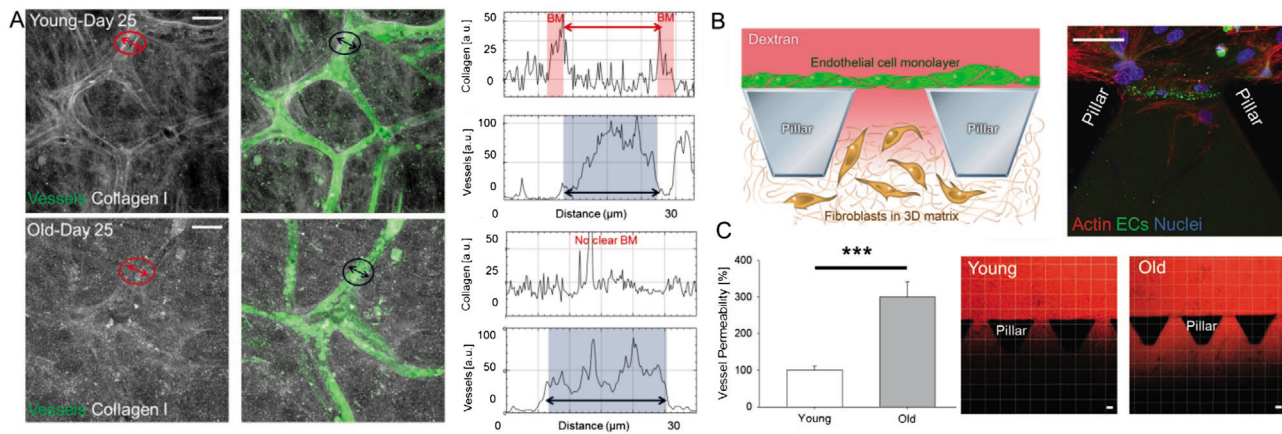


Figure 1. YFs restore structure and function of aged endothelium. A) Representative images of collagen type I (white) surrounding microvascular networks (green). Scale bars: 50 μm. Representative quantification of the intensity profile of collagen type I and vessels. Double-headed red arrows and bars indicate collagen type I peaks corresponding to BM. Double-headed blue arrows and bars represent signal from GFP-labeled vessels. At least $N = 3$ independent measurements in $N = 3$ biological replicates per condition. B) Microfluidic setup for vascular permeability measurement: schematic and immunofluorescence. dVECs: green; actin: red; nuclei: blue. Scale bar: 50 μm. C) Quantification of vascular permeability and representative images of fluorescent dextran (red) diffusion. Scale bar: 50 μm. At least $N = 15$ independent measurements in $N = 3$ biological replicates per condition (fibroblasts were obtained from $N = 5$ donors per condition). Data normalized to permeability with YFs. Student's t -test, $p < 0.001$ (***). Error bars show s.e.m. This figure refers to the skin microvasculature model.

were the result of inflammation and persistent instability^[24] of the vasculature, which was reported to induce ECM remodeling, abnormal angiogenesis and, most importantly, compromised barrier function.^[24,25] Indeed, a key feature of vascular aging is the impairment of vessel permeability.^[26] In order to test the impact of fibroblast donor chronological age on the vascular barrier, we developed a microfluidic model to create endothelial monolayers flanking 3D matrix regions with embedded YFs or OFs (Figure 1B and Figure S5, Supporting Information; methodological details are reported in the Supporting Information, Figure S6 and Movie S1, Supporting Information). We infused dextran into one chamber and quantified diffusion through the monolayer into the adjacent chamber (Figure 1C). We detected a threefold decrease in permeability when dVECs were cocultured with YFs compared to OFs ($100 \pm 11.33\%$ normalized permeability vs $299.31 \pm 41.76\%$, $p < 0.001$, at least $N = 15$ independent measurements in $N = 3$ biological replicates) (Figure 1C; Movies S2 and S3, Supporting Information). The different vascular permeability quantified in presence of YFs versus OFs suggested that the differential level of secreted factors present in the two conditions might be responsible for the activation of the endothelium and compromise its barrier function. To test this hypothesis, we analyzed the conditioned medium and found that the presence of YFs promoted a significant downregulation of IL-6 ($100 \pm 28.46\%$ normalized signal vs $162.91 \pm 7.14\%$, $p < 0.05$, fibroblasts obtained from $N = 6$ donors per condition) and CXCL10 ($100 \pm 12.50\%$ vs 161.44% , $p < 0.001$, fibroblasts obtained from $N = 6$ donors per condition) (Figure S7, Supporting Information). This point is in agreement with previous studies showing a correlation between decreased permeability and lower secretion of pro-inflammatory molecules.^[27]

Next, we wanted to study the molecular mechanisms involved in the phenotypic changes of dVECs cocultured with YFs versus OFs. We performed RNA-seq analyses on isolated dVECs that were obtained by multiple rounds of immunomagnetic-based sorting (>95% purity). The presence

of YFs had a dramatic effect on gene expression when compared to OFs. Gene ontology revealed that the presence of YFs downregulated genes associated with wound healing/smooth muscle contraction (e.g., serum amyloid A (SAA), myosin phosphatase inhibitor (*PPP1R14A*), formin-related protein (*DAAM2*), *MYL9*), biomineral tissue development/ossification (e.g., *ALPL*, *TMEM119*, *BMP4*, *LEP*), and leukocyte adhesion (e.g., *CXCL12*, *VCAM1*) (Figure 2A; Figure S8 and Dataset S1, Supporting Information). In parallel, YFs upregulated other genes associated with a negative regulation of wound healing (e.g., *PIK3CG*, *AGER*). These results suggest that YFs can limit the activation of mechanisms involved in early vascular degeneration, including the onset of pathological intercellular tension,^[28] which leads to cell–cell junction damage and impaired permeability,^[29] and vascular calcification.^[30]

A critical gene identified in our analysis is *VCAM1*, which is involved in the activation of the endothelium and subsequent leukocyte extravasation. This endothelial target was recently reported to play a critical role in neurodegeneration, since blocking *VCAM1* was able to reduce microglia activation and reverse signs of cognitive impairment.^[31] In addition, this target was identified in a large study analyzing the plasma proteomic signature of aging in healthy humans.^[32] To test if the presence of YFs could reduce the expression of *VCAM1* at the protein level, we cocultured dVECs with ten YF and ten OF cell lines. Our data show that YFs can consistently reduce the expression of this protein in dVECs ($100 \pm 14.61\%$ normalized intensity vs $142.43 \pm 15.04\%$, $p < 0.01$, fibroblasts obtained from $N = 10$ donors per condition) (Figure S9 and Table S2, Supporting Information).

Our sequencing data revealed potentially novel genes which were not previously associated with vascular aging and degeneration (e.g., *SAA*, *PPP1R14A*, *DAAM2*), suggesting that the 3D assay provides a powerful platform to study potential causes of aging. In particular, SAA has been linked with

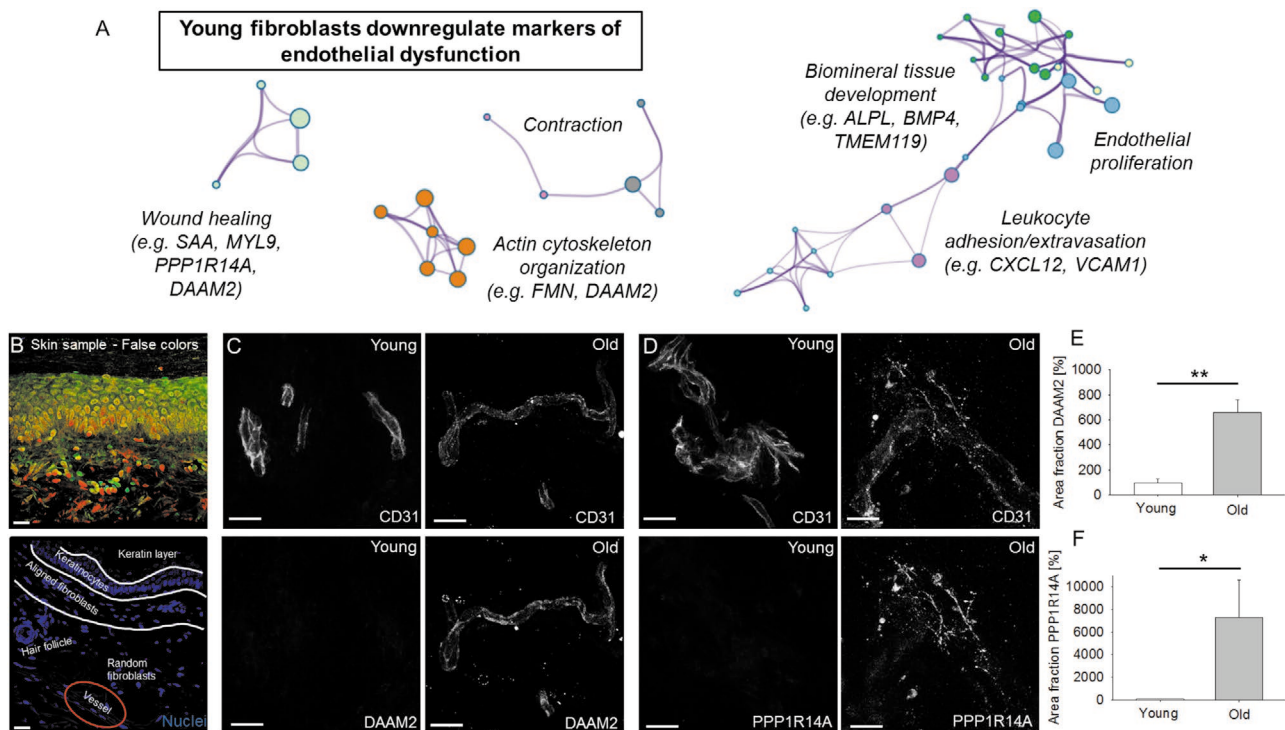


Figure 2. YFs reduce signs of vascular impairment. A) RNA-seq from isolated ECs showing downregulation of biological processes associated with wound healing and calcification in presence of YFs. Fibroblasts were obtained from $N = 5$ donors per condition. Gene ontology maps were generated with Metascape software (<http://metascape.org>). Each node represents an enriched term within a biological process (cluster). Node size is proportional to the number of genes associated with that specific node. Nodes (terms) with a similarity >0.3 are connected by edges. Edge thickness corresponds to the degree of similarity among nodes (terms). Additional details on image interpretation are available in the Experimental Section. B) Representative images of skin layers (top: false colors; bottom: nuclear staining). Representative images and quantifications of C,E) DAAM2 and D,F) PPP1R14A from biopsies of young and old donors. At least $N = 3$ tissue sections in $N = 2$ skin biopsies per age group. Data normalized to the signal in presence of YFs. Student's t -test, $p < 0.05$ (*), $p < 0.01$ (**), error bars show s.e.m. CD31 indicates endothelial cells. Scale bars: 50 μm . This figure refers to the skin microvasculature model.

inflammation^[33] and decreased expression of endothelial nitric oxide synthase, while PPP1R14A^[34] and DAAM2^[35] are involved in contractility and cytoskeleton remodeling. In order to test if the newly identified genes are biomarkers of vascular aging, we performed semiquantitative confocal microscopy on skin biopsies from individuals of different age. We collected two human skin biopsies from young and old donors (Figure 2B) and we performed immunofluorescence on tissue sections to quantify the intensity of the target signal colocalized with CD31 positive blood vessels. Consistent with the RNA-seq data, our analysis confirmed that all the identified markers were expressed at a higher level in blood vessels from old versus young donors (Figure 2C–F and Figure S10, Supporting Information). Noteworthy, the spatial quantification of the identified markers at the protein level would not be possible by simply performing immunoblotting from skin tissue lysates.

Together, these results show that YFs can partially restore the functionality of an aged endothelium by downregulating genes involved in vascular degeneration and reducing the presence of inflammatory cytokines in the vascular microenvironment. Moreover, our model recapitulates key differences between the endothelium of young and old donors, hence representing a powerful tool to identify novel aging biomarkers for the skin and potentially other organs.

2.3. Human Serum from Old Donors Compromises the Endothelial Barrier

Circulating factors discovered in the blood of young mice were shown to counteract negative effects of aging, including decline of cognitive functions.^[8] We therefore examined whether human serum might represent another promising source of candidate molecules to restore the functionality of aging tissues and blood vessels. Since YFs improved the permeability of old dVECs, we now decided to test if serum from old donors (OS) compared to serum from young donors (YS) could partially revert the improved functionality of the same dVECs. We then used microfluidic devices to create endothelial monolayers flanking 3D matrix regions containing YFs and we conditioned the medium with human serum derived from young (age range 20–30 years old) or old donors (age range 60–72 years old) ($N = 4$ donors per age group) (Table S3, Supporting Information). Strikingly, incubation with OS versus YS for at least 3 d increased vessel permeability, which was measured by quantifying fluorescent dextran diffusion through the confluent endothelial monolayer ($164.01 \pm 19.33\%$ normalized vessel permeability vs $100 \pm 13.74\%$, $p < 0.05$, at least $N = 15$ independent measurements in $N = 3$ biological replicates) (Figure 3A).

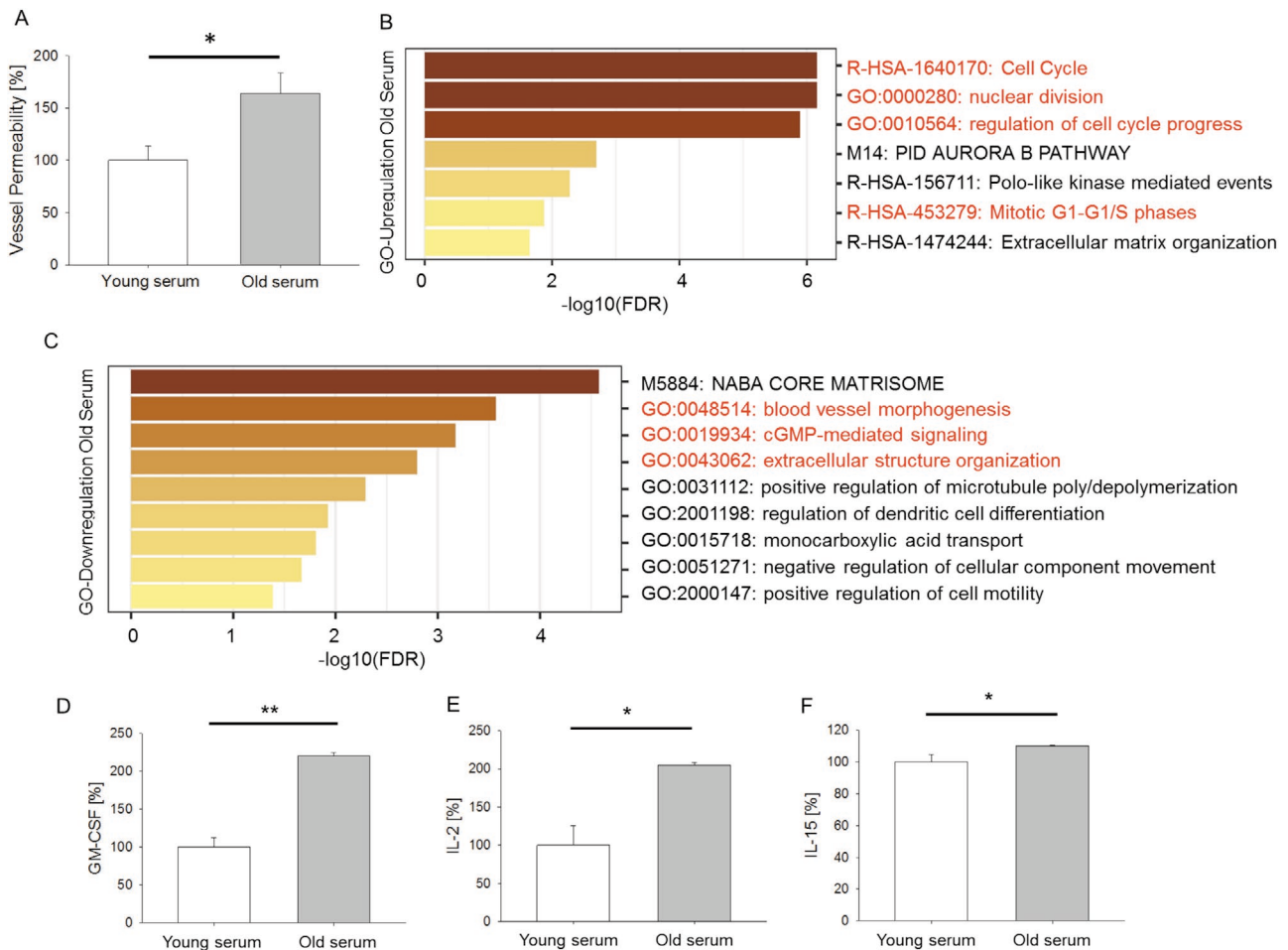


Figure 3. OS reverts the positive effect induced by YFs on the endothelium. A) OS increases vascular permeability. At least $N = 15$ independent measurements in $N = 3$ biological replicates per condition (serum was obtained from $N = 5$ donors per condition). Data normalized to permeability with YS. Student's t -test, $p < 0.05$ (*), error bars show s.e.m. B) Upregulation of biological processes with OS including cell cycle progression. Colors represent false discovery rate (FDR). Serum was obtained from $N = 4$ donors per condition. C) Downregulation of biological processes with OS including blood vessel morphogenesis and extracellular structure organization. Colors represent FDR. Serum was obtained from $N = 4$ donors per condition. D–F) Milliplex assay showing upregulation of GM-CSF, IL-2, and IL-15 with OS. Serum was obtained from $N = 5$ donors per condition. Data normalized to the amount of cytokine with YS. Student's t -test, $p < 0.05$ (*), $p < 0.01$ (**), error bars show s.e.m. This figure refers to the skin microvasculature model.

To reveal molecular mechanisms that might explain the breakdown of the barrier, we formed 3D microvascular networks embedding YFs in the presence of OS versus YS and we monitored their development over 25 d. dVECs were isolated by immunomagnetic-based sorting (>95% purity) and RNA-seq was performed. Differential expression analysis revealed that OS was sufficient to upregulate processes associated with cell cycle progression (Figure 3B and Dataset S2, Supporting Information) and to downregulate processes related to blood vessel morphogenesis and extracellular structure organization, which are typical of a healthy endothelium (Figure 3C and Dataset S2, Supporting Information). Collected data showed little overlap with differentially expressed genes in the presence of fibroblasts from donor of different ages, suggesting that serum-mediated effects might be independent from cell-mediated effects. Finally, we analyzed the culture medium from microvascular networks in culture for 25 d (Figure 3E,F and Figure S11, Supporting Information) and we observed that incubation with OS increased GM-CSF (220.44% normalized signal vs $100 \pm 12.38\%$, $p < 0.01$,

serum obtained from $N = 5$ donors per condition) (Figure 3D), IL-2 ($205.25 \pm 2.79\%$ vs $100 \pm 25.85\%$, $p < 0.05$, serum obtained from $N = 5$ donors per condition) (Figure 3E), and IL-15 ($109.93 \pm 0.68\%$ vs $100 \pm 4.48\%$, $p < 0.05$, serum obtained from $N = 5$ donors per condition) (Figure 3F). No significant changes were detected for IL-6 and CXCL10, again suggesting that fibroblasts and serum might have differential effects on dVECs.

Overall, these data highlight that our in vitro strategy can capture the intrinsic complexity associated with human serum and that incubation with OS compromises vessel functionality counteracting the positive effect of YFs.

2.4. Angiopoietin Like 4 Counteracts the Negative Effect of OS and Restores the Functionality of the Endothelium

One of the genes identified by our analysis is angiopoietin like 4 (*ANGPTL4*), which was downregulated in dVECs in presence of OS ($\log_2FC = 0.98$; $FDR = 5^{-17}$; 27th most differentially

expressed gene out of 125). We focused on *ANGPTL4* since it is a regulator of endothelial barrier functionality and previous studies have shown that it reduced signs of vascular damage and neuronal loss in mice with stroke.^[36] Importantly, we demonstrated that *ANGPTL4* is primarily expressed in blood vessels from young versus old human donors, suggesting that it might play a role in the regulation of vascular function during physiological aging (Figure S12, Supporting Information).

We therefore wanted to test if the disrupted barrier function induced by OS could be reverted by supplementing it with human *ANGPTL4*, based on concentrations previously used in vivo and in vitro ($5 \mu\text{g mL}^{-1}$).^[36,37] This concentration is higher compared to the physiological level of circulating *ANGPTL4* in humans (below $1 \mu\text{g mL}^{-1}$), even though it clearly showed protective effects in ischemic stroke. When we treated microvascular networks with OS supplemented with *ANGPTL4* compared to OS alone, we found that the integrity of cell–cell junctions was partially restored, as demonstrated by the continuous vascular endothelial (VE)-cadherin signal (Figure 4A, representative images). Quantification of VE-cadherin intensity along cell–cell junctions showed that treatment with *ANGPTL4* partially prevented the formation of junctional defects, as indicated by the VE-cadherin signal profile ($15.23 \pm 2.90\%$ normalized defect quantification vs $100 \pm 28.61\%$, $p < 0.05$, at least $N = 6$ independent measurements in $N = 3$ biological replicates per condition) (Figure 4B,C). Furthermore, we found that addition of *ANGPTL4* to OS reduced the intensity of VE-cadherin Y658 (a marker of junction disassembly) compared to OS alone ($70.76 \pm 10.4\%$ normalized fluorescence vs $100 \pm 14.77\%$, $p < 0.05$, at least $N = 3$ independent measurements in $N = 3$ biological replicates per condition) (Figure 4D,E). More intriguingly, the pattern of VE-cadherin Y658 in presence of *ANGPTL4* was more similar to the one observed with YS (Figure 4D), although the Y658 area fraction was still different compared to YS ($70.76 \pm 10.14\%$ normalized fluorescence vs $78 \pm 1.64\%$, $p < 0.01$, at least $N = 3$ independent measurements in $N = 3$ biological replicates per condition) (Figure 4E). Finally, we demonstrated that addition of *ANGPTL4* reduced vessel permeability, partially counteracting the negative effect of OS ($47.52 \pm 5.03\%$ normalized permeability vs $100 \pm 21.68\%$, $p < 0.05$, at least $N = 15$ independent measurements in $N = 3$ biological replicates per condition). Vascular permeability reached values close to those detected with YS ($47.52 \pm 5.03\%$ normalized permeability vs $29.61 \pm 3.67\%$, $p < 0.05$, at least $N = 15$ independent measurements in $N = 3$ biological replicates per condition) (Figure 4F). Confirming these findings, *ANGPTL4* overexpressing dVECs (Figure S13A, Supporting Information) showed reduced vessel permeability compared to wild type cells ($62 \pm 2.96\%$ normalized permeability vs $100 \pm 4.46\%$, $p < 0.001$, at least $N = 20$ independent measurements in $N = 3$ biological replicates per condition) (Figure 4G) and reduced expression of VE-cadherin Y658 ($57.57 \pm 3.32\%$ normalized fluorescence vs $100 \pm 27.95\%$, $p < 0.05$, at least $N = 3$ independent measurements in $N = 3$ biological replicates per condition) (Figure S13B,C, Supporting Information), indicating more stable interendothelial junctions. RNA-seq analysis performed on *ANGPTL4* overexpressing dVECs versus wild type cells (one replicate, Dataset S3, Supporting Information) suggested that *ANGPTL4* is associated with a reduced

transport of small molecules through the vascular barrier (e.g., downregulation of *AQP1*),^[38] lower vascular permeability and lower apoptosis (e.g., *CA2*),^[39] and greater potential to restore blood perfusion after ischemia (e.g., *ACE*).^[40] No significant changes were observed in terms of vascular density or vessel diameter (Figure S14, Supporting Information), suggesting that *ANGPTL4* can modulate the endothelial barrier without affecting angiogenesis/vasculogenesis.

Previous studies demonstrated that *ANGPTL4* interacts with integrin $\alpha_v\beta_3$, inhibiting Src signaling and the disruption of VE-cadherin complexes.^[36,37] Here, we extended these findings by showing that YS can specifically upregulate the expression of *ANGPTL4* in VECs and improve the barrier functionality through stabilization of adherens junctions (Figure S15, Supporting Information), therefore representing a potential target to limit the negative effects of vascular aging. However, we would like to highlight that the regulation of vascular permeability and endothelial functionality is likely multifactorial. Our finding that serum from donors of different ages can modulate the expression of *ANGPTL4* does not exclude the possibility that other mechanisms are coresponsible for the observed phenotype. Nevertheless, our approach clearly captured variations in *ANGPTL4* expression, which pushed us to test its effect on the engineered microenvironment showing that the vascular barrier can be restored through the external supply of *ANGPTL4* or the overexpression of the corresponding gene.

2.5. Serum from Patients with Alzheimer Disease Induces Transcriptional and Functional Changes to the BBB

Since our strategy was able to identify genes involved in the physiological aging of the skin microvasculature, as validated in human biopsies, we then decided to expand the scope of our assay to a more clinically relevant condition such as the BBB degeneration during AD.^[10]

A key challenge in the optimization of an in vitro 3D model of the BBB (Table S4, Supporting Information) is the identification of the optimal ratio among brain-derived VECs (bVECs), brain-derived pericytes, and astrocytes embedded in a fibrin scaffold. Current in vitro models of the BBB physically separate VECs and pericytes/astrocytes^[19] and employ induced pluripotent stem cell-derived VECs.^[21] Our system allows direct contact among cell types, which is critical for promoting physiological cell–cell interactions, and employs primary bVECs which might significantly differ compared to less mature induced cells. However, we do recognize that a continuous flow is not currently present in our model. Interestingly, we found that although the total number of cells present in the brain microvasculature model was equal or even lower than the number of cells present in the skin microvasculature model, bVECs were not able to form branched and interconnected networks until a 1:1/8:1/8 ratio with pericytes and astrocytes was set (Figure S16, Supporting Information). This difference could be due to the organ specificity of the two vascular niches. bVECs expressed typical markers of adherens (i.e., VE-cadherin) and tight (i.e., ZO-1) junctions, both at the gene (Dataset S4, Supporting Information) and protein level (Figure S16, Supporting Information). Noteworthy, a

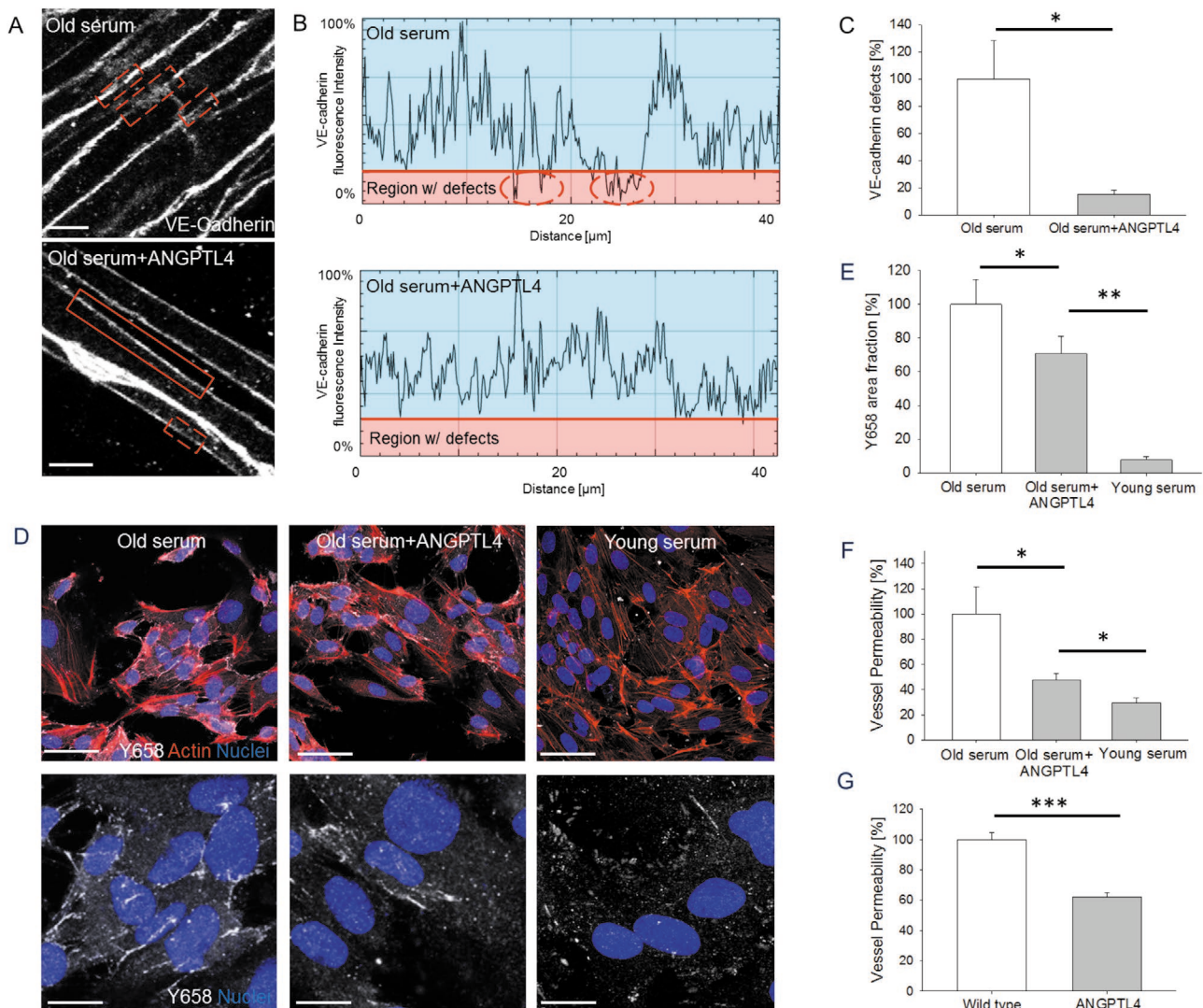


Figure 4. ANGPTL4 counteracts the negative effect of OS. **A**) Representative images of VE-cadherin staining (white) showing that discontinuous cell–cell junctions (dashed red boxes) of samples with OS can be restored (continuous red boxes) after addition of ANGPTL4. Scale bars: 10 μm . **B**) Representative images of VE-cadherin fluorescence intensity in presence of discontinuous (top graph, corresponding to dashed red boxes shown in (A)) or normal cell–cell junctions (bottom graph, corresponding to continuous red boxes shown in (A)). Light blue regions in the graphs indicate good cell–cell junctions, while red regions correspond to compromised cell–cell junctions. “Regions w/ defects” indicate experimental points with low VE-cadherin intensity, suggesting the presence of gaps. For additional details, refer to the Experimental Section. Representative images from at least $N = 6$ independent measurements in $N = 3$ biological replicates per condition. **C**) Quantification of VE-cadherin defects with OS or OS+ANGPTL4. At least $N = 6$ independent measurements in $N = 3$ biological replicates per condition. Data normalized to the signal in presence of OS. Student’s t -test, $p < 0.05$ (*), error bars show s.e.m. **D**) Representative immunofluorescence staining of VE-cadherin Y658 (white) with OS, OS+ANGPTL4, and YS. Red: actin; blue: nuclei. Scale bars: 50 μm (top images); 10 μm (bottom images). **E**) Quantification of VE-cadherin Y658 area fraction in the conditions described in (D). At least $N = 3$ independent measurements in $N = 3$ biological replicates per condition. Data normalized to the signal in presence of OS. Student’s t -test considering OS versus ANGPTL4 ($p < 0.05$ (*)) and ANGPTL4 versus YS ($p < 0.01$ (**)), error bars show s.e.m. **F**) Quantification of vascular permeability with ANGPTL4. At least $N = 15$ independent measurements in $N = 3$ biological replicates per condition. Data normalized to permeability with OS. Student’s t -test considering OS versus ANGPTL4 ($p < 0.05$ (*)) and ANGPTL4 versus YS ($p < 0.05$ (*)), error bars show s.e.m. **G**) Quantification of vascular permeability with ANGPTL4 overexpressing dVECs. At least $N = 20$ independent measurements in $N = 3$ biological replicates per condition. Data normalized to permeability with wild type dVECs. Student’s t -test ($p < 0.001$ (***)), error bars show s.e.m. This figure refers to the skin microvasculature model.

qualitative observation of the VE-cadherin pattern suggests that bVECs (Figure S16, Supporting Information) have more defined junctions compared to dVECs (Figure 4). Furthermore, clear lumens were detected throughout the whole network (Figure S16, Supporting Information), hence demonstrating a good level of maturation of the vasculature.

Recently, plasma from aged mice was reported to reduce the activity of neural progenitor cells through upregulation of endothelial VCAM1.^[31] Based on this finding and on our previous data showing that serum from young versus old donors can impair the functionality of the skin microvasculature, we hypothesized that serum from Alzheimer patients

might contain factors affecting the integrity of the BBB. To answer this question, we conditioned the BBB model with serum from Alzheimer (AS) versus age-matched healthy donors (HS) (Table S5, Supporting Information). The presence of AS increased the number of proliferating Ki-67+ cells compared to HS ($230.8 \pm 41.6\%$ vs $100 \pm 19.8\%$, $p < 0.05$, number of Ki-67+ cells normalized by the total number of cells in each region of interest). After two weeks, bVECs were immunomagnetically sorted from pericytes and astrocytes based on CD31 expression following the same methodology employed for the skin microvasculature model (purity > 95%). RNA-seq was then performed on isolated bVECs revealing a small subset of DE genes (Figure 5A and Dataset S4, Supporting Information). Surprisingly, gene set enrichment analysis (GSEA, Figure 5B and Figure S17, Supporting Information) showed that the presence of AS upregulated biological processes associated with response to VEGF stimulus, tissue migration and proliferation (Figure 5B).

Interestingly, we found downregulation of *CLDN11*, which contributes to the formation and stabilization of tight junctions, and upregulation of *PTP4A3*, a phosphatase that has been associated with increased vascular permeability.^[41] GSEA also highlighted the activation of the amyloid-beta clearance process through upregulation of *LDLR* and *DHCR24*. Importantly, human frontal periventricular white matter biopsies from Alzheimer versus age-matched healthy controls ($N = 2$ per group, Table S6, Supporting Information) costained for CD31 (i.e., vascular marker) and *PTP4A3* or *CLDN11* validated the in vitro identified targets (Figure 5D–G and Figure S18, Supporting Information). Indeed, vascular *PTP4A3* protein expression increased by more than fivefold in Alzheimer versus control tissue samples ($534.9 \pm 21.2\%$ vs $100 \pm 13.6\%$, $p < 0.001$, at least $N = 3$ tissue sections in $N = 2$ biopsies per condition), while *CLDN11* decreased by fivefold ($20 \pm 2\%$ vs $100 \pm 11\%$, $p < 0.001$, at least $N = 3$ tissue sections in $N = 2$ biopsies per condition).

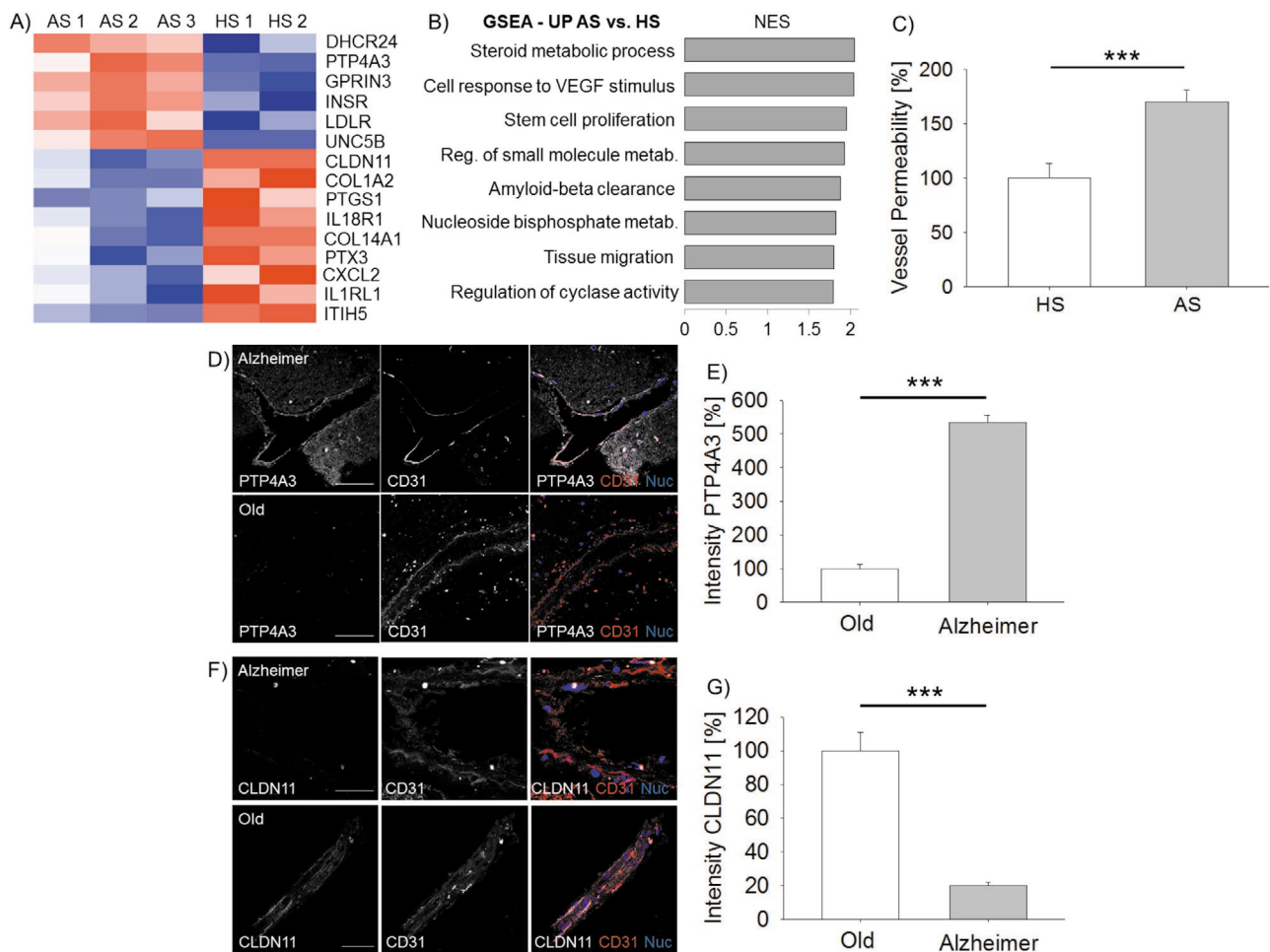


Figure 5. AS modulates bVEC gene expression and vascular permeability. A) Heat map showing DE genes in bVECs in presence of AS versus HS. Row z-score: ± 1.5 . B) Gene set enrichment analysis (GSEA) showing DE biological processes in presence of AS versus HS. C) Quantification of vascular permeability. At least $N = 25$ independent measurements in $N = 3$ biological replicates per condition (serum was obtained from $N = 3$ donors per condition). Data normalized to permeability with HS. Student's t -test ($p < 0.001$ ***), error bars show s.e.m. D–G) Validation of in vitro identified targets in human brain biopsies from Alzheimer and age-matched human donors. Representative images (D and F) and quantifications (E and G) of *PTP4A3* (D and E) and *CLDN11* (F and G) expression in blood vessels from Alzheimer and age-matched control biopsies. At least $N = 3$ tissue sections in $N = 2$ brain tissues per condition. Data normalized to the signal in age-matched control biopsies. Student's t -test, $p < 0.001$ ***, error bars show s.e.m. Scale bars: 50 μm . This figure refers to the BBB model.

To directly test if AS was able to perturb the barrier function of bVECs, we employed the same microfluidic assay previously described for the skin microvasculature model. bVECs formed a continuous monolayer which was used to study vascular permeability. Strikingly, our barrier assay demonstrated a significant increase in vascular leakiness in presence of AS versus HS ($170.20 \pm 10.91\%$ normalized vessel permeability vs $100 \pm 13.51\%$, $p < 0.001$, at least $N = 25$ independent measurements in $N = 3$ biological replicates per condition) (Figure 5C). Based on this finding, we wanted to directly test if the permeability regulator PTP4A3 was involved in the vascular leakiness observed in presence of AS. This idea is consistent with previous findings showing that PTP4A family members, including PTP4A3, are upregulated in several cancers such as ovarian, breast, and colon where they contribute to vascular leakiness, metastatic dissemination, and poor patient prognosis.^[41,42] To answer this question, AS was supplemented with the recently developed PTP4A3 inhibitor JMS-053.^[41] We found that vascular permeability was significantly decreased in presence of the inhibitor reaching values similar to HS ($98.56 \pm 6.10\%$ normalized permeability to the condition with HS) and significantly lower than AS ($196.18 \pm 8.50\%$ normalized permeability to the condition with HS) (Figure 6A). These data suggest that PTP4A3 is involved in the regulation of the BBB permeability

and that it might represent a promising target to restore its functionality during neurodegeneration. Interestingly, it is also known that members of the PTP4A family can activate RhoA by binding p115 Rho GAP and inhibiting its catalytic activity.^[43] In addition, PTP4A3 was reported to increase the amount of active RhoA^[44] and to promote Src activation,^[45] which are both associated with impaired vascular barrier. In particular, Src phosphorylation (Y416) represents a key event in the regulation of vascular permeability, since it leads to focal adhesion kinase (FAK) phosphorylation (Y576/577) and VE-cadherin phosphorylation (Y658), hence destabilizing vascular adherens junctions.^[46] We therefore tested if the observed changes in vascular permeability in presence of AS with or without PTP4A3 inhibitor (i.e., JMS-053) could be associated with the regulation of this specific biological pathway. Western blot showed that AS increased Src (Y416), FAK (Y576/577), and VE-cadherin (Y658) phosphorylation compared to HS in bVECs. This trend was partially reverted when AS was conditioned with the PTP4A3 inhibitor (Figure 6B,C). These findings suggest that PTP4A3 inhibitor might regulate bVEC barrier functionality through alteration of key phosphorylation events in permeability-regulating proteins.

Overall, we demonstrated that AS can modulate the expression of key genes involved in the functionality of the BBB. In

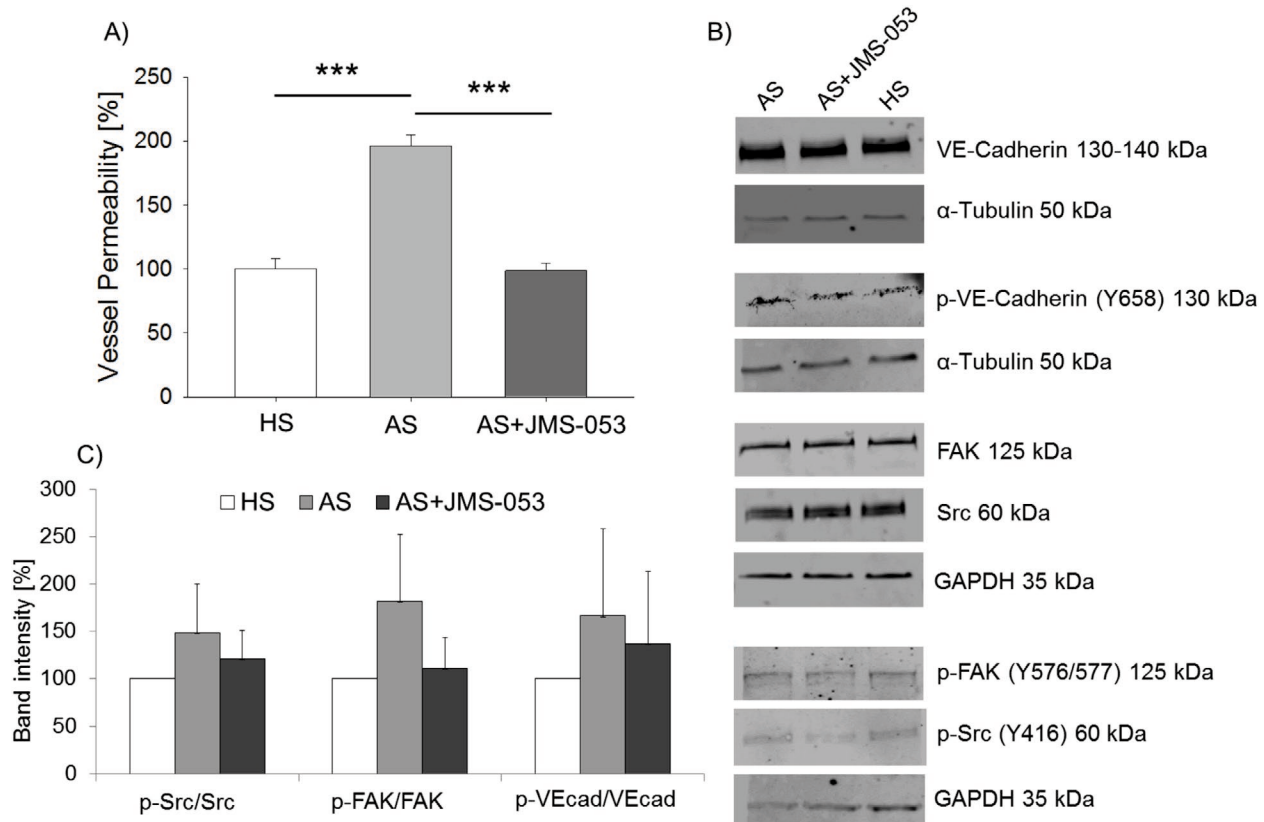


Figure 6. PTP4A3 is a key regulator of BBB functionality. A) PTP4A3 inhibitor (i.e., JMS-053) significantly reduces vascular permeability of bVECs exposed to AS, reaching a value close to the permeability of cells exposed to HS. At least $N = 60$ independent measurements in $N = 3$ biological replicates per condition (serum obtained from $N = 3$ donors per condition). Data normalized to permeability with HS. Student's t -test ($p < 0.001$ ***), error bars show s.e.m. B, C) Western blot quantification ($N = 2$ independent replicates) of Src, FAK, and VE-cadherin phosphorylation in bVECs conditioned with AS (with or without PTP4A3 inhibitor (i.e., JMS-053)) or HS. The presence of the inhibitor reduces the activation of the Src-FAK-VE-cadherin signaling axis. Error bars show s.d. This figure refers to the BBB model.

particular, we identified PTP4A3 as a potential biomarker and therapeutic target in AD by demonstrating its critical role in the regulation of the BBB permeability.

3. Discussion

We have designed and validated an in vitro strategy to test the effect of human microenvironment and serum on VECs during physiological aging and disease. To validate our approach, we initially focused our attention on a key constituent of connective tissues (i.e., skin fibroblasts) and on the effects of circulating molecules, neglecting other potentially relevant cell populations (e.g., pericytes, immune cells) and biophysical stimuli (e.g., blood flow). In this scenario, we developed and optimized our approach by only using a single donor of dVECs, mainly focusing on the reproducibility of our findings in presence of multiple fibroblasts and serum donors. Cell and serum donors were nondiabetic, nonsmokers, and without any medical issue. In addition, we would like to report that three out of four YS samples came from young, African American, female donors, while three out of four OS samples came from old, Hispanic, male donors. For this reason, collected data might also reflect racial and sex differences.

The choice to use human serum instead of plasma allows to avoid clogging issues of the microfluidic channels during barrier permeability tests. We do recognize that human serum might not contain all the circulatory factors present in human plasma and we are currently testing the possibility to perform future experiments with human plasma. However, currently available options for the use of plasma might underlie potential issues. For instance, recent studies showed that heparin is not able to fully neutralize thrombin.^[47] The presence of small amounts of thrombin can compromise the functionality of the BBB and activate astrocytes, which can in turn change the phenotype of VECs. Furthermore, the most common anticoagulant EDTA can cause VE-cadherin internalization, hence compromising the integrity of the endothelial barrier.^[48]

Our multianalytical approach combining RNA-seq, secretome screening, and functional analyses showed that YFs can revert multiple signs of vascular degeneration typical of an aged microenvironment, including BM damage, inflammation (often associated with abnormal angiogenesis), and impaired vessel permeability. Addition of OS counteracted the vascular recovery induced by YFs demonstrating that the system can be modulated by the combined effect of independent variables. We recognize that we did not test all the possible combinations of cells types (e.g., young dVECs cocultured with YFs vs OFs). Rather, we focused on the validation of the identified DE genes directly into human skin biopsies.

The skin vascular model represents a simple yet functional microenvironment which allowed us to set up a reliable strategy to analyze the emerging concept that cells or blood serum from donors of different ages can independently induce transcriptional and functional changes to blood vessels. Based on our findings using dVECs, we hypothesized that our approach could be translated to different tissues to dissect the specific role played by cells, circulating molecules, and biophysical stimuli during physiological vascular aging and pathological

remodeling. Recent evidence suggests that the contribution of microvascular dysfunction is remarkably relevant in multiple neurodegenerative diseases.^[11] In particular, we focused our attention on the BBB degeneration in AD, with the ultimate goal to identify potential targets to restore its functionality and slow down the progression of the disease. Following optimization of the 3D coculture model to take into account the organ-specific behavior of bVECs and include the basic components of the brain vascular niche, we employed our validated strategy to analyze the phenotypic change induced by AS. Importantly, the presence of AS determined a significant increase in the vascular permeability. It is important to mention that the composition of serum from AD patients might be variable (e.g., different levels of VEGF and other angiogenic factors which regulate signaling pathways affecting vascular permeability). This functional change was coupled with the identification of DE genes (e.g., *PTP4A3*, *CLDN11*, *COL1A2*) which play a critical role in the regulation of barrier functionality and vascular integrity. Indeed, it is reported that AD BBB is characterized by reduced tight junction proteins and changes in the capillary basement membrane in both cortex and hippocampus.^[10] We then focused on the specific role of PTP4A3 demonstrating that its inhibition was sufficient to restore the barrier functionality through partial normalization of the Src-FAK-VE-cadherin signaling axis. These results are in agreement with previous findings demonstrating the critical role of PTP4A3 in the regulation of the tumor vascular permeability and the metastatic spread of ovarian, breast, and colon cancer.^[41] However, we need to highlight that alternative pathways might be affected by PTP4A3 inhibition and contribute to the observed changes in vascular permeability.

RNA-seq analysis further revealed an unexpected increase in amyloid beta clearance in presence of AS (i.e., *LDLR*, *DHCR24*). While we did not investigate whether AS contains circulating amyloid beta, it is possible that the regulation of amyloid beta clearance could be one among the early protective mechanisms activated by bVECs. Indeed, it is known that the brain of AD patients switches on neuroprotective mechanisms (e.g., collagen VI production in AD may promote the sequestration of amyloid beta oligomers).^[49]

Surprisingly, GSEA analysis did not detect any signature of increased inflammation in bVECs in response to AS, with biological processes associated to IL-1 production and leukocyte migration even downregulated in presence of AS versus HS. While it is known that physiological aging is linked to tissue inflammation, it is also emerging that specific cell subpopulations differentially contribute to inflammation, complement activation, and interferon signaling. In this context, single-cell RNA-seq recently demonstrated that microglia and most importantly activated astrocytes are the main drivers of inflammation in the AD brain.^[50] Based on these findings, it would be relevant to test the model by introducing activated astrocytes or microglia from AD patients and to analyze their effect on the BBB functionality. Further, our current model primarily focused on the three major components of the brain vascular niche, without considering the contribution of neurons. Neuronal secretion of amyloid beta and the ensuing formation of amyloid deposits represent another important contribution to the alteration of the

BBB functionality.^[20] For these reasons, future studies will be focused on the characterization of the single and complementary role of circulating molecules and activated cells in the BBB degeneration.

Several attempts have been made during the last few years to analyze the effects of aging in multiple tissues, including the central nervous system^[8] and cardiac muscle.^[51] For instance, heterochronic parabiosis experiments in mice highlighted the possibility to rejuvenate the neurogenic niche through the action of GDF11.^[8] Other works suggested that young serum could restore the activity of aged endothelial progenitor cells from rats.^[52] While these studies paved the way toward the identification of novel targets, it should be considered that pathophysiological aging might be different between mice/rats and humans.^[53] Therefore, there is an increasing demand for alternative approaches which allow to study the causes and consequences of vascular aging and degeneration in a human environment. Our strategy, validated in a model of skin microvasculature and then employed to study BBB functional changes in AD, represents an important step toward this goal and could be in principle applied to study vascular changes in different organs. However, we need to highlight that a limited number of human biopsies was analyzed in our study to validate specific targets (e.g., *ANGPTL4*, *PTP4A3*). Larger cohorts of patients are required to clarify if these markers reflect specific subpopulations or represent a general indication of organ-specific vascular dysfunction. Furthermore, more mechanistic studies would be necessary to demonstrate the functional significance of other identified targets (e.g., *DAAM2*, *SAA*, *ALPL*, *PPP1R14A*) that were not fully analyzed in the present study.

The endothelium has been recently defined as “gatekeeper of homeostasis,” due to its complex network of interactions with the surrounding tissues during development, regeneration and disease.^[1] VECs are characterized by organ-specific transcriptional profiles which then determine the presence of organ-specific surface markers and different barrier functionalities.^[1,2] Hence, it is likely that the mechanisms driving vascular degeneration during aging and disease might be significantly different in each specific organ. We believe that the future introduction of additional elements involved in the vasculature pathophysiology (e.g., immune cells, blood flow, amyloid beta oligomers)^[54] could further increase the potential of this new method to identify which factors present in aged and AD blood affect vascular functionality in each organ. Furthermore, we envision the future exploitation of this approach in a preclinical setting to screen compounds targeting the aging-associated vascular degeneration.

4. Experimental Section

Cell Culture and Human Serum: The fibroblast populations (corresponding to different human donors) that were used during the experiments are reported in Tables S1 and S2 (Supporting Information). Details on the human serum used in the skin microvasculature model are reported in Table S3 (Supporting Information). Data on cells and serum samples used for the BBB model are reported in Tables S4 and S5 (Supporting Information).

RNA-seq: Library Preparation and Analysis: The RNeasy Mini kit was used to purify RNA (Qiagen). The Illumina TruSeq kit was used to

prepare cDNA libraries. The quality of the library was checked with Agilent Tape Station and the amount of cDNA quantified through Qubit. The HiSeq2500 was used to sequence the samples (single-end reading).

Reads were mapped by STAR (v2.5.3a, ref: <https://doi.org/10.1093/bioinformatics/bts635>, pmid: 23104886) to the hg19 reference genome with default parameters. Homer (v4.9.1, ref: PMID: 20513432; <http://homer.ucsd.edu/homer/>) was used to quantify the gene expression by counting the uniquely mapped reads across all exons of RefSeq genes. Genes with counts per million (cpm) > 1 for at least one-third of total samples were analyzed by edgeR [v3.20.9, ref: PMID: 22287627] for differential expression analysis. Batch effect correction was used to account for individual-specific effects on the global gene expression changes for the samples collected from human donors. Genes with adjusted *p*-value < 0.1 and absolute log fold-change > 0.5 were identified as significantly differentially expressed genes between the two treatments. Gene ontology maps were generated with Metascape software (<http://metascape.org>). GSEA was performed using WebGestaltR (v0.3., ref: <https://academic.oup.com/nar/article/47/W1/W199/5494758>) on Gene Ontology terms at cutoff of adjusted *p*-value < 0.1. Genes were ranked by the product of their negative log₁₀ transformed *p*-value and sign of fold-change.^[55]

Statistics: All quantifications were performed considering at least three independent measurements. Statistical tests (one-way ANOVA or nonpaired Student's *t*-test) were performed with Prism (GraphPad). Details on statistical tests, exact number of independent measurements, and data normalization are reported in each figure legend. Error bars represent standard error of the mean (s.e.m.), unless specified.

Data and Code Availability: Data discussed in this publication were deposited in NCBI's Gene Expression Omnibus and are accessible through GEO Series accession number GSE121444 (<https://www.ncbi.nlm.nih.gov/geo/query/acc.cgi?acc=GSE121444>).

Supporting Information

Supporting Information is available from the Wiley Online Library or from the author.

Acknowledgements

The authors greatly acknowledge R. Schulte and H. Tsai (Salk Institute) for providing fibroblasts and related protocols. The authors thank M. Schmitt (Salk Institute) and A. Ko (Millipore) for training during Milliplex assay and J. Simon (Salk Institute) for preparing illustrations. The authors thank U. Manor and S. Weiser Novak (Salk Institute) for transmission electron microscopy images. The PTP4A3 inhibitor (i.e., JMS-053) was a generous gift of Prof. P. Wipf (University of Pittsburgh) and Prof. E. Sharlow (University of Virginia). Brain biopsies were a kind gift of Prof. J. Joseph (University of Calgary). The authors also thank the Tissue Technology Shared Resource at Moores Cancer Center (La Jolla). The authors acknowledge Cooperative Human Tissue Network and Clinical and Translational Research Institute at UCSD for human skin samples. S.B. greatly acknowledges the Paul F. Glenn Center for Biology of Aging Research at The Salk Institute. R.A.D. was supported by an American Diabetes Association postdoctoral fellowship (No. 1-18-PMF-007). This research was supported by an AHA-Allen Initiative in Brain Health and Cognitive Impairment award made jointly through the American Heart Association and The Paul G. Allen Frontiers Group: 19PABH134610000. This work was supported by the National Institutes of Health Transformative Research Award grant R01 NS096786, the Keck Foundation, and the NOMIS Foundation. This work was also supported by Waitt Advanced Biophotonics Core Facility of Salk Institute with funding from NIH-NCI CCSG: P30 014195 and Waitt Foundation; NGS Core Facility and the Razavi Newman Integrative Genomics and Bioinformatics Core Facility of the Salk Institute with funding from NIH-NCI CCSG: P30 014195 and the Chapman Foundation and the Helmsley Charitable Trust.

Conflict of Interest

The authors declare no conflict of interest.

Author Contributions

S.B., R.A.D., and M.W.H. designed the study. S.B. performed experiments. L.H., M.N.S., and S.B. analyzed RNA-seq data. S.B. and M.W.H. analyzed data and wrote the manuscript.

Keywords

3D microvascular network, blood–brain barrier, endothelium, human serum, vascular aging

Received: February 5, 2020

Revised: February 21, 2020

Published online: March 17, 2020

- [1] H. G. Augustin, G. Y. Koh, *Science* **2017**, *357*, eaal2379.
- [2] M. Potente, T. Makinen, *Nat. Rev. Mol. Cell Biol.* **2017**, *18*, 477.
- [3] E. Farkas, P. G. Luiten, *Prog. Neurobiol.* **2001**, *64*, 575.
- [4] A. P. Kusumbe, S. K. Ramasamy, R. H. Adams, *Nature* **2014**, *507*, 323.
- [5] M. G. Poulos, P. Ramalingam, M. C. Gutkin, P. Llanos, K. Gilleran, S. Y. Rabbany, J. M. Butler, *J. Clin. Invest.* **2017**, *127*, 4163.
- [6] J. H. Rabe, A. J. Mamelak, P. J. McElgunn, W. L. Morison, D. N. Sauder, *J. Am. Acad. Dermatol.* **2006**, *55*, 1.
- [7] a) A. Montagne, A. M. Nikolakopoulou, Z. Zhao, A. P. Sagare, G. Si, D. Lazic, S. R. Barnes, M. Daianu, A. Ramanathan, A. Go, E. J. Lawson, Y. Wang, W. J. Mack, P. M. Thompson, J. A. Schneider, J. Varkey, R. Langen, E. Mullins, R. E. Jacobs, B. V. Zlokovic, *Nat. Med.* **2018**, *24*, 326; b) F. E. Sirianni, F. S. Chu, D. C. Walker, *Am J. Respir. Crit. Care Med.* **2003**, *168*, 1532.
- [8] L. Katsimpardi, N. K. Litterman, P. A. Schein, C. M. Miller, F. S. Loffredo, G. R. Wojtkiewicz, J. W. Chen, R. T. Lee, A. J. Wagers, L. L. Rubin, *Science* **2014**, *344*, 630.
- [9] D. A. Nation, M. D. Sweeney, A. Montagne, A. P. Sagare, L. M. D'Orazio, M. Pachicano, F. Seppehrband, A. R. Nelson, D. P. Buennagel, M. G. Harrington, T. L. S. Benzinger, A. M. Fagan, J. M. Ringman, L. S. Schneider, J. C. Morris, H. C. Chui, M. Law, A. W. Toga, B. V. Zlokovic, *Nat. Med.* **2019**, *25*, 270.
- [10] M. D. Sweeney, A. P. Sagare, B. V. Zlokovic, *Nat. Rev. Neurol.* **2018**, *14*, 133.
- [11] A. Liesz, *Science* **2019**, *365*, 223.
- [12] E. D. R. Arrojo, V. Lev-Ram, S. Tyagi, R. Ramachandra, T. Deerinck, E. Bushong, S. Phan, V. Orphan, C. Lechene, M. H. Ellisman, M. W. Hetzer, *Cell Metab.* **2019**, *30*, 343.
- [13] R. Nortley, N. Korte, P. Izquierdo, C. Hirunpattarasilp, A. Mishra, Z. Jaunmuktane, V. Kyrargyri, T. Pfeiffer, L. Khennouf, C. Madry, H. Gong, A. Richard-Loendt, W. Huang, T. Saito, T. C. Saïdo, S. Brandner, H. Sethi, D. Attwell, *Science* **2019**, *365*, eaav9518.
- [14] F. Paneni, E. Osto, S. Costantino, B. Mateescu, S. Briand, G. Coppolino, E. Perna, P. Mocharla, A. Akhmedov, R. Kubant, L. Rohrer, T. Malinski, G. G. Camici, C. M. Matter, F. Mechtigrigoriou, M. Volpe, T. F. Luscher, F. Cosentino, *Circulation* **2013**, *127*, 1229.
- [15] Y. Yoshida, Y. Hayashi, M. Suda, K. Tateno, S. Okada, J. Moriya, M. Yokoyama, A. Nojima, M. Yamashita, Y. Kobayashi, I. Shimizu, T. Minamino, *PLoS One* **2014**, *9*, e100359.
- [16] Y. Yamazaki, D. J. Baker, M. Tachibana, C. C. Liu, J. M. van Deursen, T. G. Brott, G. Bu, T. Kanekiyo, *Stroke* **2016**, *47*, 1068.
- [17] M. Cirit, C. L. Stokes, *Lab Chip* **2018**, *18*, 1831.
- [18] S. N. Bhatia, D. E. Ingber, *Nat. Biotechnol.* **2014**, *32*, 760.
- [19] B. M. Maoz, A. Herland, E. A. FitzGerald, T. Grevesse, C. Vidoudez, A. R. Pacheco, S. P. Sheehy, T. E. Park, S. Dauth, R. Mannix, N. Budnik, K. Shores, A. Cho, J. C. Nawroth, D. Segre, B. Budnik, D. E. Ingber, K. K. Parker, *Nat. Biotechnol.* **2018**, *36*, 865.
- [20] Y. Shin, S. H. Choi, E. Kim, E. Bylykbashi, J. A. Kim, S. Chung, D. Y. Kim, R. D. Kamm, R. E. Tanzi, *Adv. Sci.* **2019**, *6*, 1900962.
- [21] G. D. Vatine, R. Barrile, M. J. Workman, S. Sances, B. K. Barriga, M. Rahnama, S. Barthakur, M. Kasendra, C. Lucchesi, J. Kerns, N. Wen, W. R. Spivia, Z. Chen, J. Van Eyk, C. N. Svendsen, *Cell Stem Cell* **2019**, *24*, 995.
- [22] D. M. W. Lupa, F. Kalfalah, K. Safferling, P. Boukamp, G. Poschmann, E. Volpi, C. Gotz-Rosch, F. Bernerd, L. Haag, U. Huebenthal, E. Fritsche, F. Boege, N. Grabe, J. Tigges, K. Stuhler, J. Krutmann, *J. Invest. Dermatol.* **2015**, *135*, 1954.
- [23] J. Mertens, A. C. M. Paquola, M. Ku, E. Hatch, L. Bohnke, S. Ladjevardi, S. McGrath, B. Campbell, H. Lee, J. R. Herdy, J. T. Goncalves, T. Toda, Y. Kim, J. Winkler, J. Yao, M. W. Hetzer, F. H. Gage, *Cell Stem Cell* **2015**, *17*, 705.
- [24] M. A. Schwartz, D. Vestweber, M. Simons, *Science* **2018**, *360*, 270.
- [25] G. Eelen, C. Dubois, A. R. Cantelmo, J. Goveia, U. Bruning, M. DeRan, G. Jarugumilli, J. van Rijssel, G. Saladino, F. Comitani, A. Zecchin, S. Rocha, R. Chen, H. Huang, S. Vandekerke, J. Kalucka, C. Lange, F. Morales-Rodriguez, B. Cruys, L. Treps, L. Ramer, S. Vinckier, K. Brepoels, S. Wyns, J. Souffreau, L. Schoonjans, W. H. Lamers, Y. Wu, J. Haustraete, J. Hofkens, S. Liekens, R. Cubbon, A. Ghesquiere, M. Dewerchin, F. L. Gervasio, X. Li, J. D. van Buul, X. Wu, P. Carmeliet, *Nature* **2018**, *561*, 63.
- [26] E. F. Goodall, C. Wang, J. E. Simpson, D. J. Baker, D. R. Drew, P. R. Heath, M. J. Saffrey, I. A. Romero, S. B. Wharton, *Neuropathol. Appl. Neurobiol.* **2018**, *44*, 328.
- [27] A. Patabendige, B. D. Michael, A. G. Craig, T. Solomon, *Mol. Cell. Neurosci.* **2018**, *89*, 60.
- [28] L. A. Shehadeh, K. A. Webster, J. M. Hare, R. I. Vazquez-Padron, *PLoS One* **2011**, *6*, e25855.
- [29] M. Giannotta, M. Trani, E. Dejana, *Dev. Cell* **2013**, *26*, 441.
- [30] Y. Yao, M. Jumabay, A. Ly, M. Radparvar, M. R. Cubberly, K. I. Bostrom, *Circ. Res.* **2013**, *113*, 495.
- [31] H. Yousef, C. J. Czupalla, D. Lee, M. B. Chen, A. N. Burke, K. A. Zera, J. Zandstra, E. Berber, B. Lehallier, V. Mathur, R. V. Nair, L. N. Bonanno, A. C. Yang, T. Peterson, H. Hadeiba, T. Merkel, J. Korbelin, M. Schwaninger, M. S. Buckwalter, S. R. Quake, E. C. Butcher, T. Wyss-Coray, *Nat. Med.* **2019**, *25*, 988.
- [32] T. Tanaka, A. Biancotto, R. Moaddel, A. Z. Moore, M. Gonzalez-Freire, M. A. Aon, J. Candia, P. Zhang, F. Cheung, G. Fantoni, R. D. Semba, L. Ferrucci, *Aging Cell* **2018**, *17*, e12799.
- [33] R. He, H. Sang, R. D. Ye, *Blood* **2003**, *101*, 1572.
- [34] W. Su, Z. Xie, S. Liu, L. E. Calderon, Z. Guo, M. C. Gong, *Am. J. Physiol.* **2013**, *305*, H104.
- [35] R. Ajima, J. A. Bisson, J. C. Helt, M. A. Nakaya, R. Habas, L. Tassarollo, X. He, E. E. Morrisey, T. P. Yamaguchi, E. D. Cohen, *Dev. Biol.* **2015**, *408*, 126.
- [36] C. Bouletti, T. Mathivet, B. Coqueran, J. M. Serfaty, M. Lesage, E. Berland, C. Ardidie-Robouant, G. Kauffenstein, D. Henrion, B. Lapergue, M. Mazighi, C. Duyckaerts, G. Thurston, D. M. Valenzuela, A. J. Murphy, G. D. Yancopoulos, C. Monnot, I. Margail, S. Germain, *Eur. Heart J.* **2013**, *34*, 3657.
- [37] E. Gomez Perdiguero, A. Liabotis-Fontugne, M. Durand, C. Faye, S. Ricard-Blum, M. Simonutti, S. Augustin, B. M. Robb, M. Paques, D. M. Valenzuela, A. J. Murphy, G. D. Yancopoulos, G. Thurston, A. Galaup, C. Monnot, S. Germain, *J. Pathol.* **2016**, *240*, 461.
- [38] L. S. King, S. Nielsen, P. Agre, R. H. Brown, *Proc. Natl. Acad. Sci. USA* **2002**, *99*, 1059.

- [39] D. Torella, G. M. Ellison, M. Torella, C. Vicinanza, I. Aquila, C. Iaconetti, M. Scalise, F. Marino, B. J. Henning, F. C. Lewis, C. Gareri, N. Lascar, G. Cuda, T. Salvatore, G. Nappi, C. Indolfi, R. Torella, D. Cozzolino, F. C. Sasso, *J. Am. Heart Assoc.* **2014**, *3*, e000434.
- [40] E. A. Silva, C. Eseonu, D. J. Mooney, *Angiogenesis* **2014**, *17*, 617.
- [41] K. E. McQueeney, J. M. Salamoun, J. C. Burnett, N. Barabutis, P. Pekic, S. L. Lewandowski, D. C. Llana, R. Cornelison, Y. Bai, Z. Y. Zhang, J. D. Catrivas, C. N. Landen, P. Wipf, J. S. Lazo, E. R. Sharlow, *Oncotarget* **2018**, *9*, 8223.
- [42] A. Bardelli, S. Saha, J. A. Sager, K. E. Romans, B. Xin, S. D. Markowitz, C. Lengauer, V. E. Velculescu, K. W. Kinzler, B. Vogelstein, *Clin. Cancer Res.* **2003**, *9*, 5607.
- [43] Y. Bai, Y. Luo, S. Liu, L. Zhang, K. Shen, Y. Dong, C. D. Walls, L. A. Quilliam, C. D. Wells, Y. Cao, Z. Y. Zhang, *J. Biol. Chem.* **2011**, *286*, 42316.
- [44] J. J. Fiordalisi, P. J. Keller, A. D. Cox, *Cancer Res.* **2006**, *66*, 3153.
- [45] a) F. Liang, J. Liang, W. Q. Wang, J. P. Sun, E. Udho, Z. Y. Zhang, *J. Biol. Chem.* **2007**, *282*, 5413; b) M. W. Zimmerman, K. E. McQueeney, J. S. Isenberg, B. R. Pitt, K. A. Wasserloos, G. E. Homanics, J. S. Lazo, *J. Biol. Chem.* **2014**, *289*, 5904.
- [46] C. Jean, X. L. Chen, J. O. Nam, I. Tancioni, S. Uryu, C. Lawson, K. K. Ward, C. T. Walsh, N. L. Miller, M. Ghassemian, P. Turowski, E. Dejana, S. Weis, D. A. Cheresh, D. D. Schlaepfer, *J. Cell Biol.* **2014**, *204*, 247.
- [47] C. Puech, X. Delavenne, Z. He, V. Forest, P. Mismetti, N. Perek, *Brain Res.* **2019**, *1719*, 57.
- [48] J. S. Alexander, J. W. Elrod, *J. Anat.* **2002**, *200*, 561.
- [49] J. S. Cheng, D. B. Dubal, D. H. Kim, J. Legleiter, I. H. Cheng, G. Q. Yu, I. Tesseur, T. Wyss-Coray, P. Bonaldo, L. Mucke, *Nat. Neurosci.* **2009**, *12*, 119.
- [50] D. B. Swartzlander, N. E. Propson, E. R. Roy, T. Saito, T. Saido, B. Wang, H. Zheng, *JCI Insight* **2018**, *3*, e121109.
- [51] F. S. Loffredo, M. L. Steinhauser, S. M. Jay, J. Gannon, J. R. Pancoast, P. Yalamanchi, M. Sinha, C. Dall'Osso, D. Khong, J. L. Shadrach, C. M. Miller, B. S. Singer, A. Stewart, N. Psychogios, R. E. Gerszten, A. J. Hartigan, M. J. Kim, T. Serwold, A. J. Wagers, R. T. Lee, *Cell* **2013**, *153*, 828.
- [52] G. Zhu, M. Song, H. Wang, G. Zhao, Z. Yu, Y. Yin, X. Zhao, L. Huang, *Ann. Vasc. Surg.* **2009**, *23*, 519.
- [53] a) L. Demetrius, *Ann. N. Y. Acad. Sci.* **2006**, *1067*, 66; b) Z. Ungvari, S. Tarantini, A. J. Donato, V. Galvan, A. Csiszar, *Circ. Res.* **2018**, *123*, 849.
- [54] S. Bersini, I. K. Yazdi, G. Talo, S. R. Shin, M. Moretti, A. Khademhosseini, *Biotechnol. Adv.* **2016**, *34*, 1113.
- [55] S. Tripathi, M. O. Pohl, Y. Zhou, A. Rodriguez-Frandsen, G. Wang, D. A. Stein, H. M. Moulton, P. DeJesus, J. Che, L. C. Mulder, E. Yanguéz, D. Andenmatten, L. Pache, B. Manicassamy, R. A. Albrecht, M. G. Gonzalez, Q. Nguyen, A. Brass, S. Elledge, M. White, S. Shapira, N. Hacohen, A. Karlas, T. F. Meyer, M. Shales, A. Gatorano, J. R. Johnson, G. Jang, T. Johnson, E. Verschueren, D. Sanders, N. Krogan, M. Shaw, R. Konig, S. Stertz, A. Garcia-Sastre, S. K. Chanda, *Cell Host Microbe* **2015**, *18*, 723.